

# Transient decrease in water diffusion observed in human occipital cortex during visual stimulation

Anne Darquie<sup>\*†</sup>, Jean-Baptiste Poline<sup>\*</sup>, Cyril Poupon<sup>\*†</sup>, Hervé Saint-Jalmes<sup>‡</sup>, and Denis Le Bihan<sup>\*§</sup>

<sup>\*</sup>Service Hospitalier Frédéric Joliot, Commissariat à l’Energie Atomique, 4 Place du Général Leclerc, 91401 Orsay Cedex, France; <sup>†</sup>General Electric Medical Systems Europe, 283 Rue de la Minière, 78553 Buc Cedex, France; and <sup>‡</sup>NMR Laboratory, Centre National de la Recherche Scientifique Unité Mixte de Recherche 5012, Domaine Scientifique de la Doua, CPE, 3 Rue Grignard, 69616 Villeurbanne Cedex, France

Edited by Marcus E. Raichle, Washington University School of Medicine, St. Louis, MO, and approved May 10, 2001 (received for review March 14, 2001)

**Using MRI, we report the observation of a transient decrease of the apparent diffusion coefficient (ADC) of water in the human brain visual cortex during activation by a black and white 8-Hz-flickering checkerboard. The ADC decrease was small (<1%), but significant and reproducible, and closely followed the time course of the activation paradigm. Based on the known sensitivity of diffusion MRI to cell size in tissues and on optical imaging studies that have revealed changes in the shape of neurons and glial cells during activation, the observed ADC findings have been tentatively ascribed to a transient swelling of cortical cells. These preliminary results suggest a new approach to produce images of brain activation with MRI from signals directly associated with neuronal activation, and not through changes in local blood flow.**

Functional MRI (fMRI) has provided a powerful tool for cognitive neurosciences, offering noninvasive access to the cortical and subcortical networks involved in sensory–motor and higher-order cognitive processes on an individual basis. fMRI relies on the common principle postulated at the end of the last century by Roy and Sherrington (1) that regional blood flow and metabolism are modulated by neuronal activity. fMRI provides quantitative or qualitative maps of changes in cerebral blood flow which are interpreted, on the basis of the above principle, in terms of regions being “activated” (or sometimes “deactivated”) by sensorial, motor, or cognitive tasks. The most common approach to fMRI has been based on blood oxygen level-dependent (BOLD) contrast (2–4). During brain activation, the large increase in blood flow, which overcompensates a small increase in oxygen consumption, results in a net decrease of the blood deoxyhemoglobin concentration, which, in turn, leads to a small, but measurable, signal increase because deoxyhemoglobin is paramagnetic. Perfusion MRI techniques using contrast agents (5) or spin-magnetic-labeling methods (6) have also been used successfully. The mechanisms and the origin of the neuronal activation/blood flow relationship are still unclear, however, and are the object of many fundamental research studies (see, for example, review by Magistretti and Pellerin in ref. 7). In any case, one should bear in mind that brain activation studied with fMRI is seen through a hemodynamic window and, thus, indirectly. Furthermore, there is a delay of several seconds between the visible hemodynamic response and the onset of the neuronal response, which intrinsically limits the temporal resolution of the method. Similarly, spatial resolution is limited because the vessels at the origin of the current fMRI response feed or drain somewhat large territories compared with the activated neuronal assemblies.

Ideally, one would like to see the activity of small ensembles of neurons directly. Thus far, single-unit neuronal recordings (synaptic activity and action potentials) can be achieved in animal models or brain slice preparations and, in rare cases, intraoperatively in patients. Such studies, however, are not easy to perform and analyze, even in animals. Furthermore, only a few “units” can be recorded simultaneously in a given cortical region. In humans, electroencephalography (EEG) and magnetoencephalography (MEG) are sensitive to millisecond changes

in regional electrical activity, but the ability to resolve source localization and timing is limited by the ill-posed “inverse” problem, leading to an increasing use of EEG/MEG and fMRI in combination (8). A major advance would be the development of a noninvasive imaging method that bridges the gap between animal studies based on single-unit recordings and macroscopic human studies. Such an advance must be able to directly visualize neuronal activity (and not remote vascular effects) to precisely identify the location of the active neuronal assemblies in the cortical ribbon. Efforts in this direction have led several groups to explore new avenues for detecting neuronal activation with MRI, such as the use of calcium-analogous manganese tracers (9).

Diffusion MRI provides quantitative data on water molecular motion, a very sensitive marker of tissue structure (10). During their random, diffusion-driven displacements, water molecules probe tissue structures at a microscopic scale, well beyond the usual image resolution. The observation of these displacements thus provides valuable information on the structure and the geometric organization of tissues, such as cell size or cell orientation in space (11). MRI is the only means to observe diffusion both *in vivo* and noninvasively. The most successful application of diffusion MRI has been in brain ischemia after the discovery in the cat brain that water diffusion drops at a very early stage of the ischemic event (12). Thus, diffusion MRI can provide some patients with the opportunity to receive suitable treatment at a very acute stage, when brain tissue might still be salvageable. In addition, water molecular mobility in tissues may not be the same in all directions. This anisotropy effect results from obstacles that limit molecular movement in some directions. Diffusion anisotropy in brain white matter originates from its specific organization in bundles of more or less myelinated axonal fibers running in parallel. Diffusion in the direction of the fibers is faster than in the perpendicular direction. This feature has been exploited to map out the orientation in space of the white matter tracks (13–15).

Preliminary data have suggested that water diffusion MRI could also be used to visualize changes in tissue microstructure that might arise during large, extraphysiological neuronal activation (16). Changes in the water apparent diffusion coefficient (ADC) during neuronal activation would likely reflect transient microstructural changes of the neurons or the glial cells during activation. Observing such effects would have a tremendous impact, because they would be directly linked to neuronal events, in contrast to blood flow effects, which are indirect and remote. However, this effect, if it exists, would be extremely small (a preliminary study performed in an isolated sciatic nerve did not

This paper was submitted directly (Track II) to the PNAS office.

Abbreviations: fMRI, functional MRI; BOLD, blood oxygenation level-dependent; ADC, apparent diffusion coefficient; SPM, statistical parametric mapping; IVIM, intra-voxel incoherent motion.

<sup>§</sup>To whom reprint requests should be addressed. E-mail: lebian@shfj.cea.fr.

The publication costs of this article were defrayed in part by page charge payment. This article must therefore be hereby marked “advertisement” in accordance with 18 U.S.C. §1734 solely to indicate this fact.

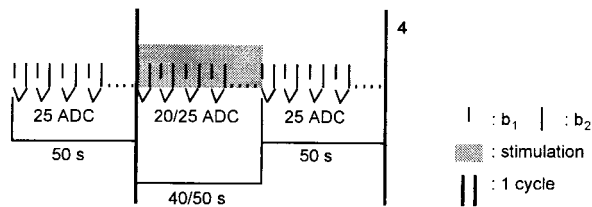


**Fig. 1.** Paradigm time course. A cycle is a 40- or 50-s visual stimulation block preceded and followed by 50-s rest periods. The cycle is repeated four or seven times. Each time point consists of a pair of images acquired sequentially with two  $b$  values ( $b_1$  and  $b_2$ ).

show any water diffusion change; ref. 17). The aim of the present work was thus to investigate whether diffusion MRI would be sensitive enough to detect activation-related neural events.

### Methods and Materials

A visual stimulation study was conducted on nine healthy volunteers (five males and four females, ages 20 to 28 years). All participants gave their informed written consent. The study was approved by an Institutional Ethic Committee (no. 95-23).

Diffusion and BOLD-sensitized imaging was performed on a whole-body 1.5-T MRI system (Signa, General Electric Medical Systems, Milwaukee, WI) equipped with an actively shielded whole-body magnetic field gradient set to allow up to  $40 \text{ mT}\cdot\text{m}^{-1}$ . An echo planar imaging sequence, sensitized to diffusion by application of additional gradient pulses on either side of the refocusing radiofrequency (RF) pulse, was used to provide images with diffusion weighting (on all three gradient axes simultaneously, so as to maintain echo time (TE) as short as possible—i.e., 72.3 ms). This sequence was run by alternating two  $b$  values ( $b \approx 200$  and  $1,443\text{--}1,461 \text{ s/mm}^2$ ) to minimize effects of motion and eddy currents, at a rate of repetition time (TR) = 1 s for a total of 758 (or 418) repetitions. The  $b$  values and the number of series and time points were set to optimize the signal-to-noise ratio in ADC images ( $\sigma_{\text{ADC}}/\text{ADC} < 0.4\%$ ). The performance of the sequence for diffusion measurement had been previously validated by using a phantom containing isopropyl alcohol at  $22^\circ\text{C}$  (18).

An alternating black-and-white flickering checkerboard (8 Hz) was used for blocks of 40 or 50 s during seven (or four) ON/OFF cycles (Fig. 1). Visual stimuli were delivered through a PC synchronized with fMRI acquisitions, using EXPE5 software (19). Three (or five) series of 8 axial slices across the calcarine fissure were acquired ( $64 \times 64$  matrix, 24-cm field of view, 4–5 mm thickness) resulting in more than 400 data points. BOLD fMRI data were also acquired with a  $T_2^*$ -weighted gradient echo planar imaging (EPI) sequence (TR = 1 s, TE = 60 ms) using the same visual stimulation paradigm, but limited to 3 ON-OFF cycles. All experimental sessions occurred in complete darkness.

Data preprocessing was performed with in-house software that corrects for image distortion induced by eddy currents in each series (15). Rigid motion effects were corrected across the three (or five) series. Statistical analysis was performed by using statistical parametric mapping (SPM) software (Friston, FIL, London; ref. 20) for both BOLD and diffusion MRI time series. ADC maps were first calculated and smoothed (kernel smoothing with full width at half maximum =  $8 \text{ mm} \times 8 \text{ mm} \times 8/10 \text{ mm}$ ). Activation-locked ADC changes were detected by using a box-car model and  $t$  test analysis. Clusters were considered significant when the associated  $P$  values were smaller than  $5 \times 10^{-3}$  ( $5 \times 10^{-2}$  after volume correction for multiple comparisons). Statistical analysis was performed considering the whole brain volume and a subset corresponding to voxels found activated in the BOLD images ( $P < 10^{-3}$ ).

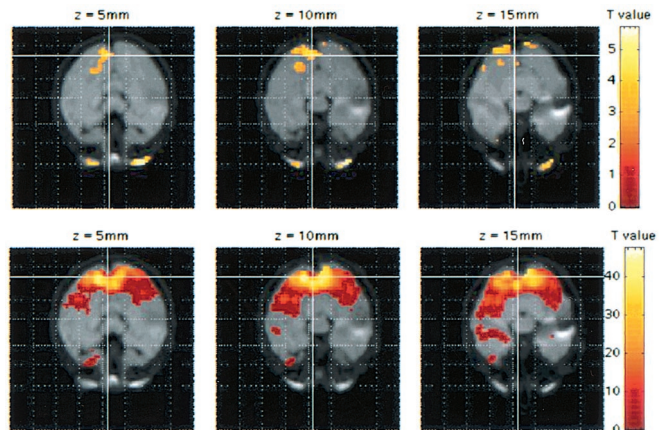


**Fig. 2.** Activation maps of one subject. These SPM maps show the location of the significantly activated voxels. (Upper) Activation maps from ADC images ( $P_{\text{corrected}} < 0.05$ ). (Lower) Activation maps from BOLD images ( $P_{\text{corrected}} < 0.001$ ).

### Results

In Fig. 2 SPM-ADC maps of three adjacent slices in one subject are shown. A large cluster (84 voxels) of significantly decreased ADC is visible in the occipital cortex within an area that also showed an activation when BOLD fMRI was used. The time course of the ADC in the most significant voxel of this cluster is shown as an example in Fig. 3. Although the baseline is very noisy, a decrease in the ADC can be seen during each visual stimulation epoch. The average ADC for each of three sequential experiments (series) for the baseline and activated conditions are shown in Fig. 4. On average over the 3 runs, the baseline ADC is  $0.676 \times 10^{-3} \text{ mm}^2/\text{s}$  and significantly diminishes to  $0.664 \times 10^{-3} \text{ mm}^2/\text{s}$  during stimulation (i.e., a 1.79% decrease). To better visualize the ADC change, the ADC time course was averaged over the four activation blocks for each individual run and then smoothed by using a five-point moving-average algorithm (Fig. 5). The shape of the ADC time-response differs from the BOLD fMRI signal time course, in particular by a slow return to baseline. However, the moving average used for the ADC precludes any fine analysis of the ADC response time. Furthermore, the actual time resolution for the ADC images was 2 s (instead of 1 s for the BOLD images) because of the interleaved  $b_1/b_2$  acquisition process.

This pattern of ADC change was observed in the visual cortex of four participants, with cluster sizes varying between 12 and 84 voxels. The ADC decrease (Table 1) was always small (0.78% in

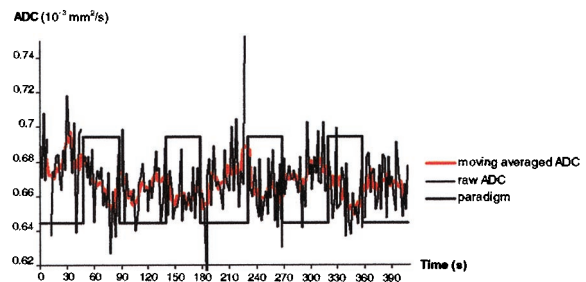


**Fig. 3.** Example of raw ADC time course. This plot shows the time course of the ADC during one series in the most significantly activated cluster of Fig. 2 (raw data, no averaging of repeated protocols). This plot highlights the degree of noise in the data, although a trend of decreased ADC can be observed for each stimulation block (made more visible by using a moving average).

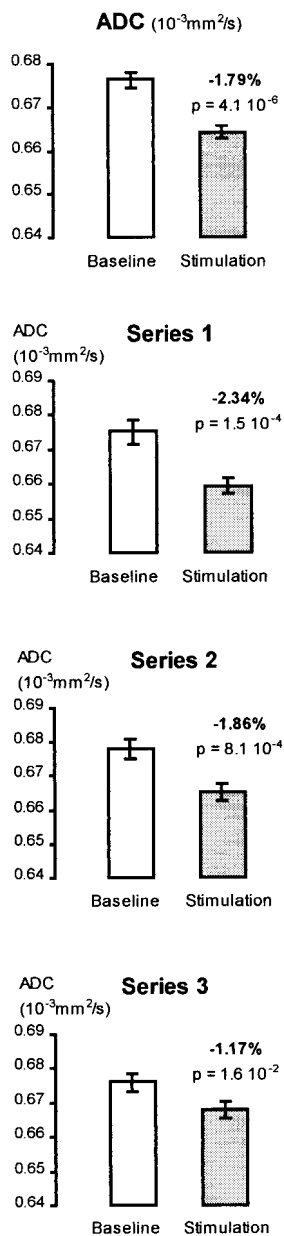


**Fig. 4.** ADC changes. These histograms show the average ADC values ( $\pm$ SD on the average) in the baseline and activated conditions for 3 sequential runs (series of four ON/OFF cycles) of the same participant (all changes are significant at  $P < 10^{-3}$ ). For the stimulated condition the ADCs were calculated by averaging the 10 center points of each activation block. The baseline ADCs were obtained from the 10 points preceding the first activation block. The overall ADC change averaged over the three series is shown in the histogram at the top.

average), but always significant except in one participant, for whom the ADC decrease remained less than the statistical significance threshold after volume correction ( $P_{\text{corrected}} \approx 0.1$ ). Three subjects did not show any significant change in the ADC. In the remaining two subjects, strong paradigm-correlated residual movement artifacts in diffusion-weighted images prevented any analysis.

## Discussion

In this paper we report the first observation, to our knowledge, of a decrease in the ADC occurring transiently in cortex during

physiological activation. This effect was seen in the human visual cortex of healthy participants stimulated by a black and white 8-Hz-flickering checkerboard. The ADC decrease was small ( $<1\%$ ) and required optimizing data acquisition parameters to improve signal-to-noise ratio and accuracy on ADC measurements (below 0.4%), and powerful statistical analysis to be revealed. However, the ADC change observed in clusters of several voxels lying within the BOLD activated region was significant and reproducible, and closely followed the time course of the activation paradigm. The fact that the population of voxels where a significant decrease in ADC was observed was much smaller than the subset of voxels considered as activated on BOLD images likely results from differences in sensitivity (BOLD statistical threshold in Fig. 2 has been slightly lowered compared with most fMRI studies to approach ADC significance threshold). Also, the mechanisms of the two approaches are likely different (see below) and relative contrast-to-noise ratios of the two methods cannot yet be directly compared.

The introduction of diffusion-weighted MRI in the field of brain activation imaging is not entirely novel, but it has been used in a different context. Our first attempt arose from the prospect that at very low  $b$  values (less than  $100 \text{ s/mm}^2$ ) diffusion-weighted MRI could be sensitive to the displacement of water molecules in a pseudorandomly orientated capillary network [intra-voxel incoherent motion (IVIM) imaging; ref. 21] and, thus, blood microcirculation. The BOLD method developed years later proved to be much more sensitive and reliable, because the IVIM method requires a very high signal-to-noise ratio in the raw images (22). Several groups have recently obtained brain activation maps with IVIM MRI, detecting increases of up to 50% of the ADC in stimulated human visual cortex (23). This effect is still linked to a hemodynamic response, but the IVIM approach is potentially useful to sort out the flow and oxygenation contributions to the BOLD response that occurs during brain activation. This IVIM effect can also be used “negatively” to eliminate from the BOLD data the blood vessel contribution. By inserting small gradient pulses in a BOLD sensitized MRI sequence, one may “crush” the signal component arising from the blood flowing in a pseudorandom manner in each voxel, giving emphasis to the tissue component of the BOLD response (23). This flow-suppressing effect occurring at very low  $b$  values ( $<20 \text{ s/mm}^2$ ) has also been used in the context of perfusion MRI using arterial spin labeling methods (24). In the present work, the  $b$  values were chosen above the main IVIM sensitivity range, so as to avoid any contamination by flow effects.

At intermediate  $b$  values (lower than  $700 \text{ s/mm}^2$ ) an increase of the ADC has also been observed during visual stimulation by Zhong *et al.* (25). The mechanism responsible for this increase has been ascribed to a change in local internal magnetic field gradients. These local gradients result from the susceptibility difference that exists between tissues and vessels filled with red cells containing paramagnetic deoxyhemoglobin (26, 27). Hence, the local  $b$ -value depends on the local concentration of deoxyhemoglobin, which in turn is modulated by the brain activation status. Because this local  $b$ -value is not known, the ADC calculation gives a value artifactually modulated by these local gradients. Theoretical models and simulations have shown that a decrease in deoxyhemoglobin content (as observed with BOLD fMRI during activation) leads to the observed apparent increase of the ADC. Here also, the ADC time course is expected to closely follow the vascular BOLD signal time course.

In the present work, much larger  $b$  values were used ( $b = 1,461 \text{ s/mm}^2$ ). One cannot at this stage completely rule out that the decrease in the ADC we have seen could result partially from a residual susceptibility-related signal drop predominating in the images acquired at  $b = 200 \text{ s/mm}^2$ . Only further experiments designed to demonstrate that the time course of the ADC change does not match that of the hemodynamic BOLD response, as

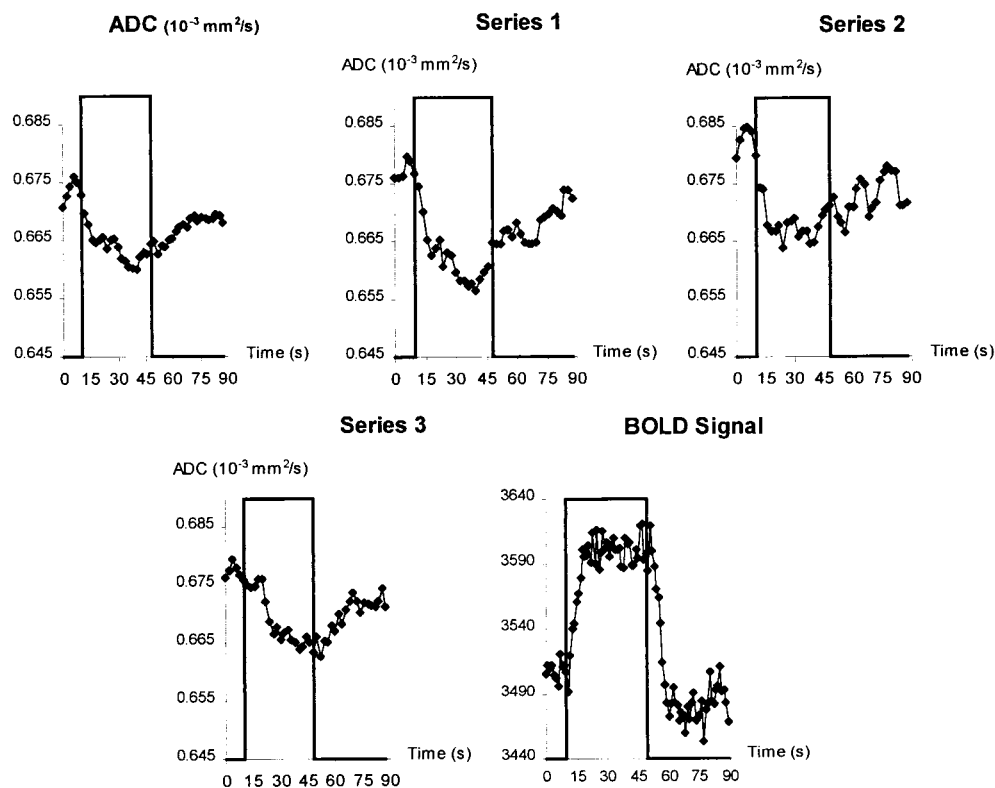


**Fig. 5.** Averaged ADC time courses. The raw ADC time courses acquired over the four ON/OFF cycles of each series were averaged and smoothed by using a five-point moving average. The first plot corresponds to the ADC obtained from the three series averaged together. For comparison the averaged BOLD signal time course is shown in the last panel (arbitrary units).

suggested in some of our data (Fig. 5), would ultimately resolve this issue. However, with our current settings we have not yet been able to perform those experiments, which would require much higher acquisition rates while keeping adequate signal-to-noise ratio. It seems, therefore, that the transient ADC drop we have observed is truly a water diffusion slowdown concomitant with cortical stimulation. Several experimental observations and models support the idea that water diffusion might decrease during brain activation. Extracellular water diffusion in the brain is exquisitely sensitive to changes in cell size. Changes in cell volume induced by osmotic agents are accompanied by changes in water diffusion (an increase in cell diameter resulting in a decrease ADC and vice versa) (28–31). So far, the best-known example of an ADC decrease linked to cell swelling is brain ischemia, where the ADC decreases at a very early stage in the infarcted areas (12, 32). This ADC decrease has been linked to cytotoxic edema and the associated cell swelling that results from the failure of the Na/K cellular membrane pump. Although the exact mechanism has not yet been firmly established, it seems

that the main effect comes from the increase in tortuosity in the extracellular space that results from the cell swelling and the associated increase in the diffusion path for water molecules (33). This concept has been validated in tissue preparations by directly monitoring diffusion of extracellular tracers, such as tetramethylammonium, by using ion-sensitive microelectrodes (34). Within the range of  $b$  values used in this study, water in the extracellular compartment predominates in the ADC, although exchange effects between the intracellular and extracellular are certainly present (18, 35).

Several groups using animal models have reported a decrease of the ADC during status epilepticus induced by bicuculline (16) or when cortex is overstimulated (36). The change in ADC propagates along the cortex at a speed of about 1–3 mm/min in line with the so-called spreading depression (37–41). Here also the decrease in ADC has been ascribed to cell swelling and increased extracellular tortuosity induced by this intense neuronal activity (42). In the cat cortex, transient changes in ionic transmembrane fluxes, especially  $K^+$ , are accompanied by the movement of water and cellular swelling caused partly by osmotic imbalance (43).

Early studies based on optical measurements in animal preparations have identified an early change in photon scattering that occurs immediately at the onset of the stimulation, and well before changes are seen in the oxy/deoxyhemoglobin spectra (44). Although the mechanisms for these changes in photon scattering have not been fully elucidated yet, changes in neuronal volume, especially at the axon hillock, have been put forward (44). More recent optical imaging techniques in tissue preparations, as well as *in vivo* techniques, have confirmed the existence of intrinsic regional changes in light transmittance during stimulation of synaptic pathways, which can be attributed to cell swelling occurring at the site of action potential initiation (45).

**Table 1. Statistics on the activated clusters detected in four participants**

Subject no.	No. of voxels in each cluster	ADC change, %		
		Averaged*	Largest	Smallest
1	84* (50) <sup>†</sup>	−1.40	−2.34	−0.70
2	27* (27) <sup>†</sup>	−0.78	−1.26	−0.50
3	12 (11) <sup>†</sup>	−0.47	−0.69	−0.12
4	14 (6)	−0.50	−0.75	−0.10

\*Significant on the whole volume ( $P < 0.001$  and  $P_{\text{corrected}} < 0.05$ ).

<sup>†</sup>Significant on the BOLD-activated volume ( $P < 0.001$  and  $P_{\text{corrected}} < 0.05$ ).

Interestingly, it seems that this swelling also involves dendrites and glial cells, although the mechanisms could be different (46) and the changes could last longer for glial cells (47). It is also worth noting that contractile proteins associated with dendritic spines (in which the majority of synapses are located in the cerebral cortex) could allow these spines to change rapidly in shape during neuronal activity (48, 49). However, these spines occupy a very small volume fraction.

It is important to point out that the link between cell swelling and decreased ADC is the associated decrease of the extracellular space fraction, which always appears to be correlated with an increased tortuosity for water diffusion (50) and an ADC decrease. The increase of the relative fraction of the less mobile, intracellular water pool might also contribute to the ADC decrease. This ADC modulation thus directly reflects changes in the geometric arrangement of the neurons and glial cells found in the brain neuropil. This arrangement differs in peripheral nerves, suggesting, perhaps, the reason why no diffusion changes could be observed in the stimulated sciatic nerve (17), as the nerve does not contain any neuronal cell bodies, axon hillocks, or dendrites. Also, the myelination of many of the axons in the nerve might limit swelling of the axons because of the tight wrapping of the Schwann cells around the axons. This would also be true for heavily myelinated tracts in the brain. On the other

hand, based on the work of Anderson *et al.* (29), the 0.8% ADC decrease we have observed would correspond to a 1–1.6% change in cell volume.

Finally, one cannot fully eliminate the possibility that ADC changes could result from temperature changes. It has also been suggested that brain temperature could drop locally by 0.2–1°C, during activation (51). As the sensitivity of diffusion to temperature is about 2.4% per degree Celsius (52), our observed diffusion drop would be compatible with such a temperature decrease. The time dependence of this possible temperature change, which is awaiting confirmation (temperature increases have also been seen), would, however, follow the metabolic (BOLD) response.

Although it is not possible to firmly ascribe our observed ADC changes to variations in cortical cell geometry by using our data, in the light of other reports our findings suggest an avenue in the field of brain activation imaging that could provide the opportunity to directly observe signals associated with neuronal activation and not through blood flow. These preliminary results enhance the great potential for functional studies of diffusion MRI, which already allows neuronal connections to be visualized through white matter fiber tracking algorithms (13–15).

We thank Ken Moya, Ph.D., for his insightful comments and his editorial assistance.

1. Roy, C. W. & Sherrington, C. S. (1890) *J. Physiol.* **11**, 85–108.
2. Kwong, K. K., Belliveau, J. W. & Chesler, D. A. (1992) *Proc. Natl. Acad. Sci. USA* **89**, 5675–5679.
3. Bandettini, P. A., Wong, E. C., Hinks, R. S., Tikofski, R. S. & Hyde, J. S. (1992) *Magn. Reson. Med.* **25**, 390–397.
4. Ogawa, S., Tank, D. W., Menon, R. S., Ellerman, J. M., Kim, S. G., Merkle, H. & Ugurbil, K. (1992) *Proc. Natl. Acad. Sci. USA* **89**, 5951–5955.
5. Belliveau, J. W., Kennedy, D. N., McKinstry, R. C., Burchbinder, B. R., Weisskoff, R. M., Cohen, M. S., Vevea, J. M., Brady, T. J., Rosen, B. R. & Buchbinder, B. R. (1991) *Science* **254**, 716–719.
6. Edelman, R. R., Siewert, B., Darby, D. G., Thangaraj, V., Nobre, A. C., Mesulam, M. M. & Warach, S. (1994) *Radiology* **192**, 513–520.
7. Magistretti, P. J. & Pellerin, L. (1999) *Med. Sci.* **15**, 451–456.
8. Liu, A. K., Belliveau, J. W. & Dale, A. M. (1998) *Proc. Natl. Acad. Sci. USA* **95**, 8945–8950.
9. Lin, Y. J. & Koretsky, A. P. (1997) *Magn. Reson. Med.* **38**, 378–388.
10. Le Bihan, D. (1995) *NMR Biomed.* **8**, 375–386.
11. Latour, L. L., Svoboda, K., Mitra, P. P. & Sotak, C. H. (1994) *Proc. Natl. Acad. Sci. USA* **91**, 1229–1233.
12. Moseley, M. E., Cohen, Y. & Mintorovitch, J. (1990) *Magn. Reson. Med.* **14**, 330–346.
13. Conturo, T. E., Lori, N. F., Cull, T. S., Akbudak, E., Snyder, A. Z., Shimony, J. S., McKinstry, R. C., Burton, H. & Raichle, M. E. (1999) *Proc. Natl. Acad. Sci. USA* **96**, 10422–10427.
14. Mori, S., Kaufman, W. E., Pearlson, G. D., Crain, B. J., Stieltjes, B., Solaiyappan, M. & Van Zijl, P. C. (2000) *Ann. Neurol.* **47**, 412–414.
15. Poupon, C., Clark, C. A., Frouin, V., Regis, J., Bloch, I., Le Bihan, D. & Mangin, J. F. (2000) *Neuroimage* **12**, 184–195.
16. Zhong, J., Petroff, O. A. C., Prichard, J. W. & Gore, J. C. (1993) *Magn. Reson. Med.* **30**, 241–246.
17. Gulani, V., Iwamoto, G. A. & Lauterbur, P. C. (1999) *Magn. Reson. Med.* **41**, 241–246.
18. Clark, C. A. & Le Bihan, D. (2000) *Magn. Reson. Med.* **44**, 852–859.
19. Pallier, C., Dupoux, E. & Jeannin, X. (1997) *Behav. Res. Methods Instr. Comput.* **29**, 322–327.
20. Friston, K. J., Jezzard, P. & Turner, R. (1994) *Hum. Brain Mapp.* **1**, 153–171.
21. Le Bihan, D., Breton, E., Lallemand, D., Aubin, M. L., Vignaud, J. & Laval Jeantet, M. (1988) *Radiology* **168**, 497–505.
22. Le Bihan, D., Turner, R., Moonen, C. T. W. & Pekar, J. (1991) *J. Magn. Reson. Imaging* **1**, 7–28.
23. Song, A. W., Wong, E. C., Tan, S. G. & Hyde, J. S. (1996) *Magn. Reson. Med.* **35**, 155–158.
24. Ye, F. Q., Mattay, V. S., Jezzard, P., Frabk, J. A., Weinberger, D. R. & McLaughlin, A. C. (1997) *Magn. Reson. Med.* **37**, 226–235.
25. Zhong, J., Kennan, R. P., Fulbright, R. K. & Gore, J. C. (1998) *Magn. Reson. Med.* **40**, 526–536.
26. Does, M. D., Zhong, J. & Gore, J. C. (1999) *Magn. Reson. Med.* **41**, 236–240.
27. Kennan, R. P., Zhong, J. & Gore, J. C. (1995) in *Diffusion and Perfusion Magnetic Resonance Imaging: Application to Functional MRI*, ed. Le Bihan, D. (Raven, New York), pp. 110–121.
28. Loubinoux, I., Volk, A., Borredon, J., Guirimand, S., Tiffon, B., Seylaz, J. & Meric, P. (1997) *Stroke* **28**, 419–426.
29. Anderson, A. W., Xie, J., Pizzonia, J., Bronen, R. A., Spencer, D. D. & Gore, J. C. (2000) *Magn. Reson. Imaging* **18**, 689–695.
30. O'Shea, J. M., Williams, S. R., van Bruggen, N. & Gardner-Medwin, A. R. (2000) *Magn. Reson. Med.* **44**, 427–432.
31. Hsu, E. W., Aiken, N. R. & Blackband, S. J. (1996) *Am. J. Physiol.* **271**, C1895–C1900.
32. Warach, S., Chien, D., Li, W., Ronthal, M. & Edelman, R. R. (1992) *Neurology* **42**, 1717–1723.
33. Nicholson, C. & Sykova, E. (1998) *Trends Neurosci.* **21**, 207–215.
34. Vorisek, I. & Sykova, E. (1997) *J. Cereb. Blood Flow Metab.* **17**, 191–203.
35. Niendorf, T., Dijkhuizen, R. M., Norris, D. G., Van Lookeren Campagne, M. & Nicolay, K. (1996) *Magn. Reson. Med.* **36**, 847–857.
36. Zhong, J., Petroff, O. A. C., Pleban, L. A., Gore, J. C. & Prichard, J. W. (1997) *Magn. Reson. Med.* **37**, 1–6.
37. Busch, E., Gyngell, M. L., Eis, M., Hoehn Berlage, M. & Hossmann, K. A. (1996) *J. Cereb. Blood Flow Metab.* **16**, 1090–1099.
38. Hasegawa, Y., Latour, L. L., Formato, J. E., Sotak, C. H. & Fisher, M. (1995) *J. Cereb. Blood Flow Metab.* **15**, 179–187.
39. Latour, L. L., Hasegawa, Y., Formato, J. E., Fisher, M. & Sotak, C. H. (1994) *Magn. Reson. Med.* **32**, 189–198.
40. Mancuso, A., Derugin, N., Ono, Y., Hara, K., Sharp, F. R. & Weinstein, P. R. (1999) *Brain Res.* **839**, 7–22.
41. Röther, J., De Crespigny, A. J., D'Arcueil, H. & Moseley, M. E. (1996) *J. Cereb. Blood Flow Metab.* **16**, 214–221.
42. Hansen, A. J. & Olsen, D. R. (1980) *Acta Physiol. Scand.* **108**, 355–365.
43. Dietzel, I., Heinemann, U., Hofmeier, G. & Lux, H. D. (1980) *Exp. Brain Res.* **40**, 432–439.
44. Cohen, L. B. (1973) *Physiol. Rev.* **53**, 373–418.
45. Andrew, R. D. & MacVicar, B. A. (1994) *Neuroscience* **62**, 371–383.
46. Ransom, B. R., Yamate, C. L. & Connors, B. W. (1985) *J. Neurosci.* **5**, 532–535.
47. Svoboda, J. & Sykova, E. (1991) *Brain Res.* **560**, 216–224.
48. Crick, F. (1982) *Trends Neurosci.* **5**, 44–47.
49. Halpain, S. (2000) *Trends Neurosci.* **23**, 141–146.
50. Chen, K. C. & Nicholson, C. (2000) *Proc. Natl. Acad. Sci. USA* **97**, 8306–8311. (First Published July 11, 2000; 10.1073/pnas.150338197)
51. Yablonskiy, D. A., Ackerman, J. J. H. & Raichle, M. E. (2000) *Proc. Natl. Acad. Sci. USA* **97**, 7603–7608.
52. Le Bihan, D., Delannoy, J. & Levin, R. L. (1989) *Radiology* **171**, 853–857.